

Measurement of a High-Temporal Resolution Arterial Input Function from MR Projections: Extension to Radial Acquisition to Compensate for Local Tissue Enhancement

Jen Moroz¹, Stefan A Reinsberg¹, and Piotr Kozlowski^{2,3}

¹Physics and Astronomy, University of British Columbia, Vancouver, BC, Canada, ²Radiology, UBC, University of British Columbia, BC, Canada, ³UBC MRI Research Centre, University of British Columbia, BC, Canada

Target Audience: This abstract is geared towards individuals who perform Dynamic Contrast-Enhanced Magnetic Resonance Imaging (DCE-MRI) in an animal model and analyze the data with an arterial input function (AIF).

Purpose: DCE-MRI has become an increasingly popular technique for studying tumours¹ due to known differences in their vascular structure.² Quantitative analysis is often performed through pharmacokinetic (PK) modelling;³ but this requires that the contrast agent concentration is known temporally in both the blood (referred to as the arterial input function (AIF)) and in the tissue of interest.⁴ The AIF is difficult to measure in mice owing to their small body size, rapid heart rates, and limited number of sufficiently large vessels.

Our group has shown that the AIF may be measured, with high temporal and spatial resolutions, with a series of MR projections.⁵ However, this technique assumes that the contrast agent remains intra-vascular. This limitation may be overcome by utilizing a radial acquisition scheme. Radial data has the advantage that each projection can be used to estimate the AIF, and a subset of these projections may be used to quantify and correct for local tissue enhancement from a time-series of MRI images.

Methods: This study was based on computer simulations. A simple image was created to resemble a mouse tail; this involved a circular phantom of radius fifty pixels, and a small vessel, of radius five pixels, located near the edge (Fig 1). The phantom phase was set to zero, while the phase of the vessel was determined from a previously measured projection-based AIF.⁵ An intensity gradient was applied to the phantom to approximate data acquisition from a surface coil. Local contrast perfusion into the tissue surrounding the vessel, referred to as tissue enhancement, was added to the image for 2330 frames. The magnitude of enhancement was calculated from the change in the tissues T_1 (assuming $T_{10} = 1000$ ms, $r_1 = 3.6$ (mM s)⁻¹ for Gd-DTPA at 7 T,⁶ and a FLASH experiment with a flip angle of 30°), while the phase of enhancement was determined from the concentration of contrast agent in each pixel.^{5,7} Radial projections were obtained by applying a forward radon transform to the images. Projections were selected temporally to approximate Golden angle sampling⁸ for 233 unique angles (angular increment 111.245° or 72°*(360°/233 projections per repetition)). Gaussian white noise was added to the projections.

The projection-based AIF requires that the background signal is known, so that it may be subtracted from the acquired projection. To achieve this aim for each unique angle, radial images were reconstructed using the non-equidistant fast Fourier Transform (NFFT)⁹ with a Fibonacci number of pre-injection ($N_{pre}=233$) projections ($N = 34, 55, 89, 144$ or 233). The reconstruction angle was defined as the modulus of the difference between the angle of the first and i -th projections in the image subset. Background profiles were calculated by first setting the vessel signal to zero, then projecting the image along the direction of phase encode (second dimension). Signal from the vessel was extracted from the projections by subtracting the background profile, at angle i , from the projection at angle i . The AIF was calculated following three steps: first, the average phase of the pixels corresponding to the vessel was determined, then the phase difference from the average pre-injection phase was calculated, and finally the phase difference was converted into a concentration using our scanners calibration factor.⁵

Correction for tissue enhancement was performed with a sliding window reconstruction¹⁰ (A Fibonacci number of projections was used in the reconstruction and a sliding window width of floor(# projections used / 5)). The vessel signal was zeroed and the NFFT images were projected along the direction of phase-encode. A background correction profile was obtained by comparing the time-series projections with the corresponding pre-injection background profile. The background correction profile was added (complex) to the acquired projections. Finally, a projection-based AIF was estimated from the corrected profiles following the method described above. A temporal resolution of 100 ms / projection was used to match experiments.

Results: Fig 2 compares the expected input AIF (black), the initial uncorrected AIF (green) and the tissue enhancement corrected AIF (magenta). The uncorrected AIF agrees with the expected curve at the peak, but deviates from expectations beyond 70 s. After correcting for tissue enhancement, the AIF is in better agreement with the expected curve beyond 70 s (<6% error), but underestimates the concentration at the peak by up to 9.3%. The underestimation of the peak increases when more radial projections are used in the reconstruction, likely a result of temporal blurring. The RMS error is a factor of 2.7-5.2 smaller with the correction is applied.

Discussion: The use of radial sampling is advantageous for a projection-based AIF as each projection serves as a single AIF data point, and may be used in the reconstruction of a radial image to assess local tissue enhancement. The NFFT reconstruction algorithm produces good quality images – defined by its ability to reproduce the original image, and having minimal image artifacts – with as few as 55 radial projections. Further compression to 34 projections showed signs of streaking artifacts, particularly when the enhancement region was large. The correction greatly reduced the bias from tissue enhancement, with NFFT reconstructions with 55 or 89 projections producing the best results. The correction also appears to have reduced the noise floor of the AIF, though the oscillating behaviour is still present.

Both radial AIFs show an oscillating pattern. The relative contribution of the total signal from the vessel is small, therefore it is possible that these oscillations stem from varying partial volume effects for images constructed at different reference angles. It is advisable to use an AIF-specific surface coil with a high sensitivity, so that a larger number of pixels are used to estimate the concentration and partial volume effects are reduced.

The in-vivo AIF shown in our previous work⁵ may suffer from local tissue enhancement.

Because it was acquired with Cartesian sampling, it is unclear which time points are affected, and by how much. Radial sampling has two major advantages for our technique: first, local tissue enhancement may be quantified and corrected for, and the NFFT images may validate the AIF measurement beyond the peak.

Radial imaging with a sliding window approach is attractive as images may be constructed with a number of temporal resolutions. By comparing image series with different temporal resolutions, it is possible to gain further insights into the nature (size and rate of growth) of the enhancement region. At the peak of enhancement in the vessel, the contrast agent concentration is varying rapidly and local tissue enhancement is expected to be minimal. The projection-based AIF is well suited here as it can capture these rapid changes with minimal bias from local enhancement. NFFT images following injection will serve as a tool to help determine when the AIF should be corrected.

Conclusion: This study shows that the measurement of a high-temporal resolution AIF may be enhanced with radial sampling when a projection-based approach is used. Radial data allows the investigation of how local tissue enhancement may affect the signal, and compensate for it. The corrected AIFs resemble the expected result, but underestimates the concentration at the peak.

References: 1. Yankeelov T.E. and Gore J.C., *Curr Med Imaging Rev.* 1:3(2):91-107 (2009). 2. Taylor et al, *JMRI*.10:903-907 (1999). 3. Rijpkema et al, *JMRI*. 14:457-463 (2001). 4. Ragan et al, *NMR Biomed.* 24:373-384 (2011). 5. Moroz et al, *MRM*. 2013 Feb 14. 6. Yankeelov et al, *MRI*. 23:519-529 (2005). 7. Cron et al, *MRM*. 66:498-504 (2011). 8. Lin et al, *MRM*. 60:1135-1146 (2008). 9. Keiner et al, *ACM Trans Math Software*. 36:1-30 (2009). 10. Adluru et al, *MRM*. 57:1027-1036 (2007).

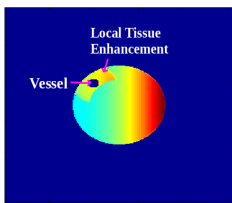


Fig 1:

Magnitude image of the simulated mouse tail phantom.

Average Phase of Vessel from Radial Projections

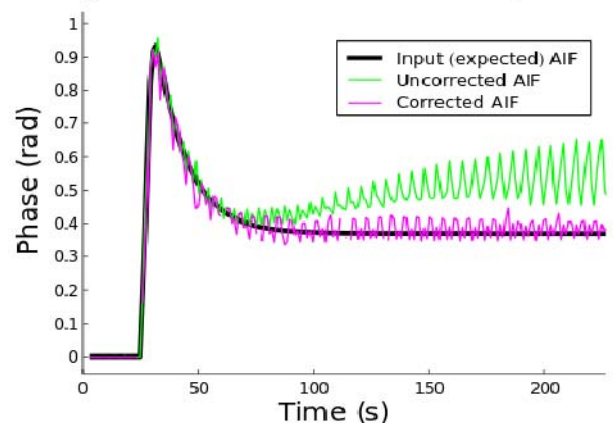


Fig 2: Comparing the expected AIF (black), the uncorrected AIF (green), and the tissue-enhancement corrected AIF (magenta). NFFT correction images were constructed with 55 radial projections.